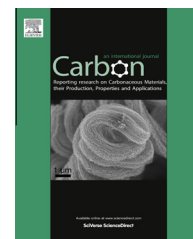


Available at www.sciencedirect.com

ScienceDirect

journal homepage: www.elsevier.com/locate/carbon

Electron-beam engineering of single-walled carbon nanotubes from bilayer graphene

Gerardo Algara-Siller ^{a,b}, Adriano Santana ^c, Rosalind Onions ^c, Mikhail Suyetin ^c, Johannes Biskupek ^a, Elena Bichoutskaia ^c, Ute Kaiser ^{a,*}

^a Group of Electron Microscopy of Materials Science, Central Facility for Electron Microscopy, Ulm University, Albert-Einstein-Allee 11, 89081 Ulm, Germany

^b Department of Chemistry, Ilmenau Technical University, Weimarer Str. 25, 98683 Ilmenau, Germany

^c School of Chemistry, University of Nottingham, University Park, Nottingham NG7 2RD, UK

ARTICLE INFO

Article history:

Received 10 February 2013

Accepted 31 July 2013

Available online 6 August 2013

ABSTRACT

Bilayer graphene nanoribbons (BGNRs) with a predefined width have been produced directly from bilayer graphene using a transmission electron microscope (TEM) in scanning mode operated at 300 kV. The BGNRs have been subsequently imaged in high-resolution TEM mode at 80 kV. During imaging, the interaction of the electrons with the sample induces structural transformations in the BGNR, such as closure of the edges and thinning, leading to the formation of a single-walled carbon nanotube (SWCNT). We demonstrate using molecular dynamics simulations that the produced SWCNT is, in fact, a flattened SWCNT with elliptical circumference. Density functional theory calculations show that the band gap of the flattened semiconducting SWCNTs is significantly smaller than that of the undeformed semiconducting SWCNTs, and this effect is particularly profound in narrow SWCNTs.

© 2013 Elsevier Ltd. All rights reserved.

1. Introduction

The properties of graphene, strongly depend on its morphology, which are determined by the size, shape, temperature, and boundary conditions [1]. This presents excellent opportunities for using structural modifications of graphene at the atomic scale to modify its physical and chemical properties. Most successful examples of simple geometrical tailoring of the graphene structure include the formation of quasi-one-dimensional graphene nanoribbons (GNRs) by lithographic methods [2,3] or surface-assisted coupling of molecular precursors [4], and nanoscrolls by electrostatic deposition of graphene under controlled gas environments [5] or induced scrolling by isopropyl alcohol [6]. GNRs in particular feature remarkable size- and edge-dependent electronic properties

due to the quantum confinement and lattice symmetry [7]. The armchair-edged GNRs, for instance, have width-dependent energy gaps, while the zigzag-edged GNRs are always metallic with a localized state at the edge when the electron spin is unpolarized [8,9]. Furthermore, the controlled modification of the structure of graphene and its properties has been achieved by means of electromagnetic fields [10], hydrogenation [11], fluorination [12,13], oxidation [14–16], ion irradiation [17,18], adsorption of individual molecules [19], interior and exterior doping [20–22] and electron irradiation [23].

Transmission electron microscopy (TEM) has been a key tool to characterize low-dimensional carbon nanostructures. For instance, aberration-corrected high-resolution TEM (AC-HRTEM) experiments on graphene confirmed at the atomic

* Corresponding author.

E-mail address: ute.kaiser@uni-ulm.de (U. Kaiser).

0008-6223/\$ - see front matter © 2013 Elsevier Ltd. All rights reserved.

<http://dx.doi.org/10.1016/j.carbon.2013.07.107>

scale that graphene monolayers are stabilized through the formation of out-of-plane ripples, which maintain the planar morphology thus avoiding a collapse into folds or nanoscrolls [24]. Also, recent AC-HRTEM studies have shown that a wide range of carbon nanostructures can be obtained by nanoengineering single and multilayered graphene with a high-energy electron beam (e-beam) [25,26]. The effects of bond stretch and strain become very significant during e-beam induced transformations of carbon nanostructures [27]. Thus, a correlation between the local deformation of carbon bonds (and the graphene morphology in general) and its impact on the properties [28] are key considerations to nanoengineer graphene and related materials using AC-HRTEM. In this paper, we present a new example of nanoengineering bilayer graphene (BG) with a careful selection and combination of the e-beam parameters leading to the formation of a flattened SWCNT within the large BG (BG-SWCNT).

2. Materials and methods

2.1. Graphene fabrication and transfer

BG was fabricated using micromechanical cleavage method [29] deposited on 90 nm SiO₂. The BG flake was selected by analyzing its optical contrast [30] then, transferred to a gold Quantifoil grid (Quantifoil GbmH, Jena, Germany) via potassium hydroxide [31]. The sample was subsequently annealed on air to 200 °C for 10 min and inserted in to the TEM.

2.2. Scanning TEM and AC-HRTEM

For our experiments we used an imaging-side aberration-corrected TITAN 80–300 (FEI, Netherlands). First we nanoengineered a BGNR within the BG using 300 kV scanning TEM nanoprobe with emission of 48 μA, dwell time 13 μs and camera length of 0.160 m under ambient conditions. We cutout sets of always two parallel lines on the BG by line scanning, and verified the completeness of the cut through both layers of the BG by annular dark field imaging. As a result, we obtained BGNR with lengths between 20 and 70 nm and widths of 5–10 nm. Then, we characterized our system by 80 kV AC-HRTEM. The microscope parameters used for AC-HRTEM imaging were: spherical aberration of 20 μm at Scherzer conditions. The electron beam current density during imaging was $1.88 \times 10^6 \text{ e}^-/\text{nm}^2 \text{ s}$. Image series were taken with 1 s exposure with an interval between frames of 2 s. Under these conditions the graphene lattice is resolved and so the structure can be directly interpreted.

2.3. Theoretical simulations

The GULP program [32] has been employed for the constant temperature molecular dynamics (MD) simulations using the bond-order Brenner empirical potential [33] and for structure optimization using the ReaxFF potential of van Duin and co-workers [34], in which distance-dependent bond-order functions are used to represent the contributions of chemical bonding to the potential energy. MD calculations were run at

$T = 2500 \text{ K}$, with the equilibration time of 5 ps, the production time of 200 ps, and the simulation time step of 1 fs.

Electronic structure calculations of undeformed and uniformly flattened SWCNTs were performed using density functional theory with semiempirical dispersion corrections (DFT + D) as implemented in CASTEP 5.5 simulation code [35]. The Perdew-Wang (PW91) [36] parametrization of the generalized gradient approximation (GGA) was used to describe the exchange-correlation energy, and van der Waals interactions were included using the OBS semiempirical dispersion corrections [37] to the total GGA/PW91 energies. An “on-the-fly” pseudopotential generator has been used to eliminate the core states and describe the valence electrons by nodeless pseudo-wave functions. The Brillouin zone was sampled with $(1 \times 1 \times 6)$ Monkhorst-Pack k -point grid. A plane wave basis set with the cutoff energy of 400 eV and an orthorhombic unit cell with dimensions $(25 \times 25 \times 4.26) \text{ \AA}^3$ were used. The radial deformation, or flattening, of SWCNT was achieved by applying stress along the y -axis to the opposite sides of the SWCNT cross-section, which causes squeezing of SWCNT in the y -direction and elongation in the x -direction. The degree of flattening is defined by a dimensionless parameter $f = (R_x - R_y)/R_x$, known as ellipticity. The geometry of flattened SWCNTs were relaxed with remnant forces of less than 0.01 eV/\AA .

3. Results and discussion

3.1. AC-HRTEM

Fig. 1a shows an 80 kV AC-HRTEM image of an e-beam nanoengineered BGNR of $5 \pm 0.5 \text{ nm}$ width and about 20 nm in length. In the middle part the BGNR has a constriction (BGNR-constriction) of 3.2 nm in width marked by blue arrows (although the constriction is not deliberately introduced, in almost all experiments on nanoengineering bilayer graphene the constrictions in a BGNR appeared during 80 kV imaging). After nanoengineering the BG some small flat graphene flakes, shown by black arrows, remain on the surface of the BG and BGNR. Various adsorbates, marked by green arrows, can be also seen due to their dark contrast. In this initial image, most of the edges of BG and BGNR are already closed as identified by the strong edge contrast [38,39].

Recently, the e-beam induced displacement cross-section for graphene has been accurately measured and theoretically explained including thermal vibrations [40]. Hence, the probability to remove three-coordinated bulk-like carbon atoms from defect-free graphene with 80 keV electrons is low but it can create bond rotations [41], sputter atoms from a site near a topological defect [42], or displace carbon atoms at an open edge of graphene [43]. Therefore, in the course of imaging, the BGNR thins down and reconstructs using the plentiful source of carbon atoms from the sample. Another process involved in the structure transformation of BGNR during AC-HRTEM experiments is the chemical etching of carbon atoms due to their interaction with adsorbates [44]. The edges of BG and BGNR, once closed, adopt a semitubular structure [45], so it is expected that the closed edges have a threshold energy for atom removal close to that of a SWCNT, therefore the

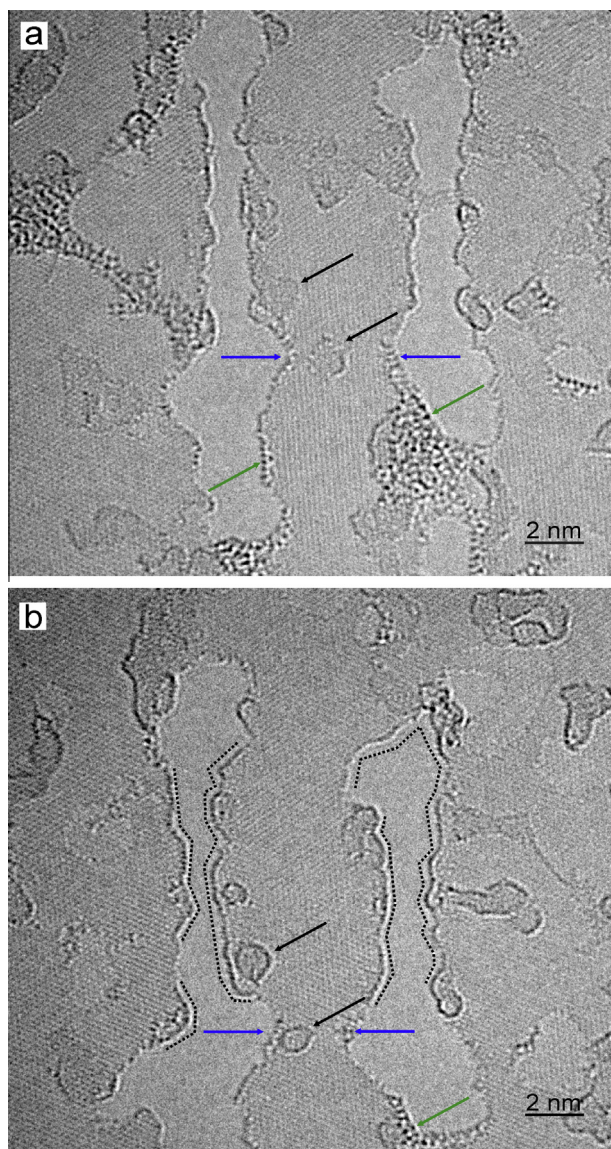


Fig. 1 – (a) Initial AC-HRTEM image of a nanoengineered BGNR; blue arrows point to a BGNR-constriction with open edges, smallest width 3.2 nm; green arrows point to adsorbates at the edges of the BGNR; black arrows point to small flat graphene flakes located on top of BGNR. (b) BGNR after an accumulated dose of $4.32 \times 10^8 \text{ e}^-/\text{nm}^2$ showing a reduced width of the BGNR-constriction, $2.2 \pm 0.2 \text{ nm}$, (blue arrows); closed edges of BGNR and BG are seen by the stronger edge contrast (dotted lines); green arrow points to remaining adsorbates; some small flat graphene flakes transformed to fullerene-like cages on top of closed-edge BG and BGNR, marked by black arrows.

structural changes at the edges under the e-beam are driven mostly by knock-on damage mechanisms [46].

Fig. 1b presents an image after an accumulated dose of $4.32 \times 10^8 \text{ e}^-/\text{nm}^2$ showing that the BGNR-constriction has thinned down to a width of $2.2 \pm 0.2 \text{ nm}$ (blue arrows). Here, most of the edges in the structure have already fully zipped (see the dotted black lines) but some remnant atoms from

the contamination continue to interact chemically with carbon atoms at the edges (green arrows).

Most of the small flat graphene flakes found on top of BGNR and BG underwent transformations and formed hollow graphitic structures (shown by black arrows). These hollow graphitic structures, e.g. fullerenes, are formed in AC-HRTEM through the continuous bond rotation and displacement of atoms by the e-beam [47].

The continuous e-beam irradiation results in a pronounced reduction of the BGNR-constriction (Fig. 2a) followed by the formation of a closed-edge BGNR-constriction (Fig. 2b). In Fig. 2a the BGNR-constriction has a width range of 1.5–2.0 nm with a single layer graphene extension. Fig. 2b shows that the edges of the BGNR and BGNR-constriction have closed entirely. At this stage of transformation the width of the closed-edge BGNR-constriction is 1 nm in its wider part and 0.7 nm at the thinnest section with sharp kinks at the edges. The sharp kinks at the edges require a pentagon-heptagon pair formation [38] or vacancies to interconnect each intersecting point. Hence, the carbon atoms at these sites are easier to be displaced. The closed-edge BGNR-constriction suffers further atom removal and reconstruction. As shown in Fig. 2c, this reconstruction has formed a $0.9 \pm 0.1 \text{ nm}$ wide closed-edge BGNR-constriction with smooth edges. Following the image sequence, we show in Fig. 2d the thinnest closed-edge BGNR-constriction. This closed-edge BGNR-constriction of 0.5 nm in width appears after an accumulated dose of $1.44 \times 10^9 \text{ e}^-/\text{nm}^2$. The sequence of images shown in Fig. 2 confirms that AC-HRTEM with the 80 keV e-beam allows modification of a carbon nanostructure while simultaneously atomically imaging the dynamics of carbon structures.

3.2. Theoretical calculations

The structural transformation of the nanoengineered BGNR under the continuous e-beam irradiation has been modeled using MD simulations as described in Section 2.3. The modeling approach adopted here is similar to that proposed in [48] where radiation damage dynamics has been explicitly included in HRTEM image simulations. The e-beam induced loss of carbon atoms at the edge destabilizes BG and BGNR structures as it increases the number of dangling bonds at the edges. The subsequent edge reconstruction, which involves the formation of pentagons and local curvature, brings covalently deficient carbon atoms closer to each other. This promotes the formation of new carbon bonds across the layers of BG and BGNR leading to zipping of the edges through the reduction of the number of dangling bonds. This is a thermodynamically favorable process, which has a profound stabilizing effect leading to the total closure of the edges and formation of a closed-edge BG and BGNR. This result is in good agreement with previous theoretical results on the open edge reconstruction of double-walled carbon nanotubes [49].

For the case of a closed-edge BGNR (Fig. 3a), the structure is predicted to have fractional nanotubes formed at the edges with an optimum radius of curvature strongly dependent on the width of the initial BGNR [45], this structure can be described as a collapsed nanotube. A closed-edge BGNR with greater width experiences stronger van der Waals interaction, and fractional nanotubes with smaller radii are formed at its

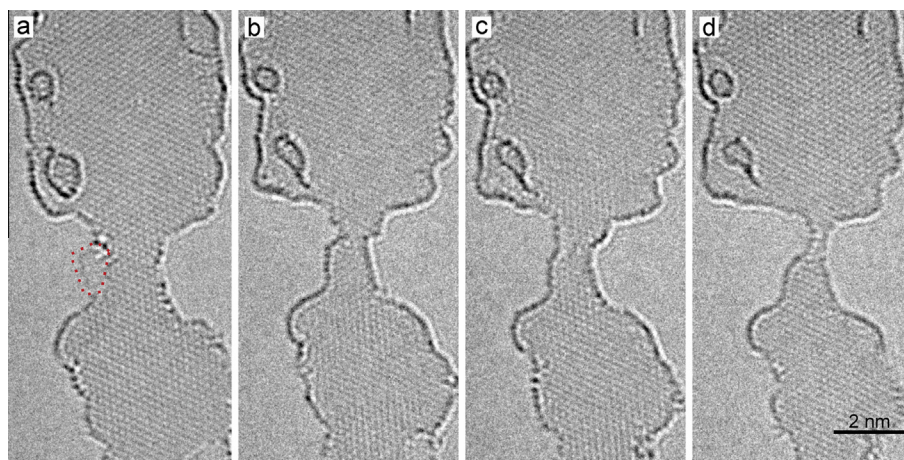


Fig. 2 – AC-HRTEM images with accumulated dose of: (a) $9.7 \times 10^8 \text{ e}^-/\text{nm}^2$, (b) $1.10 \times 10^9 \text{ e}^-/\text{nm}^2$, (c) $1.2 \times 10^9 \text{ e}^-/\text{nm}^2$, (d) $1.44 \times 10^9 \text{ e}^-/\text{nm}^2$. (a) closed-edge BGNR and a BGNR-constriction (1.5–2.0 nm width). The BGNR-constriction has opened edges and an extension of single-layer graphene (marked by the red dotted line). (b) The edges the BGNR-constriction have thinned down and closed with sharp kinks. (c) Reconstruction under the e-beam to a smooth closed-edge BGNR-constriction (thinnest section of 0.9 nm). (d) This closed-edge BGNR-constriction thinned down to 0.5 nm width before breaking (not shown). (For interpretation of the references to colour in this figure legend, the reader is referred to the web version of this article.)

edges [50,51]. Fig. 3a presents a model closed-edge BGNR of 5.7 nm in width, which was optimized using a classical Dreiding-like force field [52]. In agreement with Liu et al. [38] we have found that near the closed edges bilayer graphene exhibits AA stacking, and it is only at a distance of approximately 1.8 nm away from the edge that bilayer graphene adopts the most common AB stacking of Bernal graphite.

The red highlighted areas in Fig. 3b,c depict the closed-edge sections of a BGNR, to which the closed-edge BGNR-constriction is attached. In our simulations, the width of these closed-edge BGNRS segments is 3.8 nm. After geometry optimization, these segments also adopt the AA-layer stacking, which are consistent with Fig. 3a and the observations of Liu et al. [38]. The AA-layer stacking near the edge is therefore triggered by the formation of the closed edges in order to reduce the local near-edge strains. Our simulations confirm that the closed-edge bilayer graphene segments are held together by the attractive van der Waals forces. The predicted structures shown in Fig. 3b and c match closely the experimental images presented in Fig. 2c and d. These simulations further reveal that the 0.9 nm and 0.5 nm wide closed-edge BGNR-constrictions, attached to the closed-edge segments of bilayer graphene, are fully formed SWCNTs but flattened and having ellipsoid shape in circumference. The degree of flattening is governed by the overall strain induced by the closed-edge BNGR and BG and by the long-range van der Waals attraction.

The wider SWCNT, Fig. 3b, has the higher degree of flattening $f=0.23$. To further elucidate the effect of the van der Waals interactions on the e-beam engineering of BG-SWCNTs we carry out MD simulations on an extremely narrow SWCNT shown in Fig. 3c. As expected, the resulting structure has a smaller degree of flattening $f=0.12$. Thus, the van der Waals interactions within the closed-edge BGNR and BG dominate and affect even the structures with diameters close to the lower stability limit for pristine SWCNTs [23].

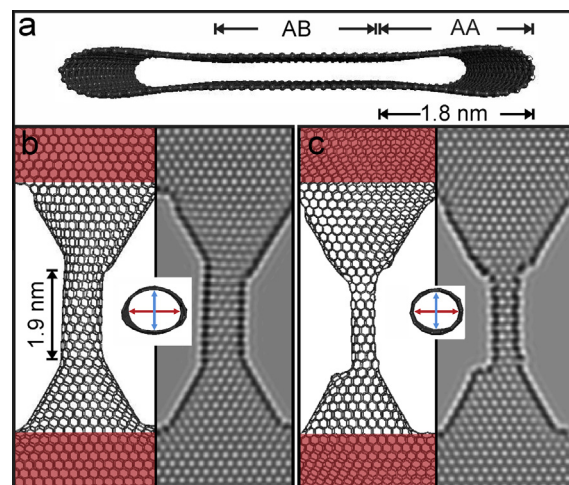


Fig. 3 – (a) An example of a modeled closed-edge BGNR of 5.7 nm in width obtained with a classical force-field optimization. Graphene sheets remain parallel with closed edges described as fractional nanotubes. This closed-edge BGNR shown in figure (a) can be seen in the MD simulations in the red highlighted areas in figures (b and c). (b) (left) MD simulated BG-SWCNT. The SWCNT has elliptical circumference having a major axis of $0.92 \pm 0.02 \text{ nm}$ (shown in the inset by red delimiter), and a minor axis of $0.71 \pm 0.02 \text{ nm}$ (blue delimiter), with a degree of flattening of $f=0.23$; (b) (right) TEM image calculation using QSTEM package [53] of the modeled structure. (c) (left) MD simulation of the thinnest experimentally found BG-SWCNT with a major axis of $0.57 \pm 0.02 \text{ nm}$ and a minor axis of $0.50 \pm 0.02 \text{ nm}$ (shown in inset), with degree of flattening of $f=0.12$; (c) (right) corresponding TEM image calculation. These simulations correspond to the experimental BG-SWCNTs presented in Fig. 2c and d, respectively. (A colour version of this figure can be viewed online.)

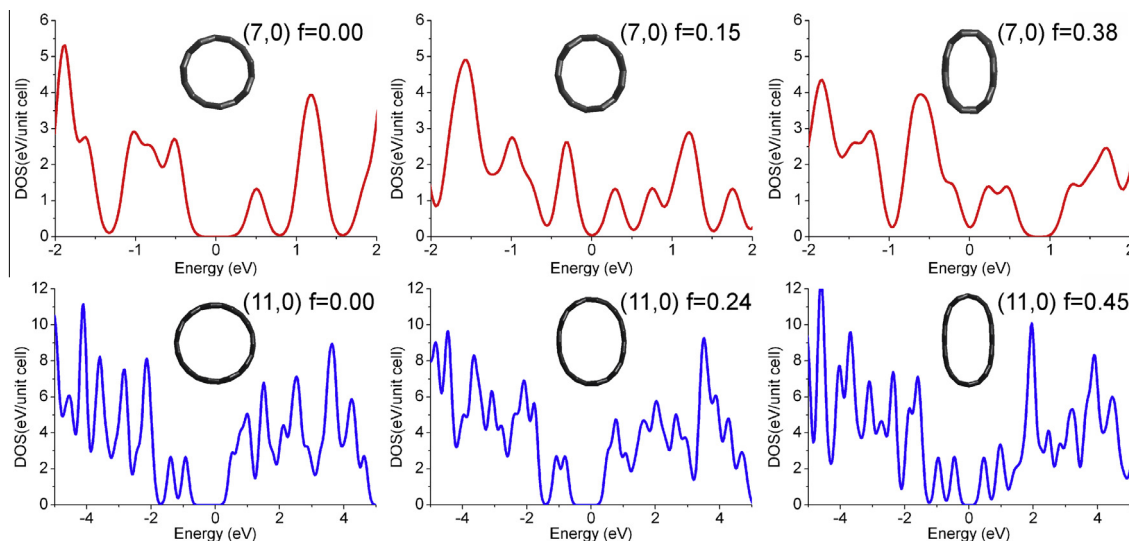


Fig. 4 – DFT density of states calculations. **Top (red)** a (7,0) SWCNT with variable degree of flattening: left, $f = 0$ (pristine nanotube) with a band gap of 0.5 eV; center, $f = 0.15$ with a band gap of 0.1 eV; right, $f = 0.38$ leading to metallization. **Bottom (blue)** a (11,0) SWCNT: left, $f = 0$ (pristine nanotube) band gap of 0.9 eV; center, $f = 0.24$ with a band gap of 0.8 eV; right, $f = 0.45$ with a band gap of 0.4 eV. (A colour version of this figure can be viewed online.)

The initial width of a BGNR is essential for the atomic scale e-beam engineering of BG-SWCNT as the electronic properties of the SWCNT depend very strongly on the degree of flattening [54–56]. Fig. 4 presents DFT calculations, as implemented in CASTEP quantum chemistry package [57], of the density of states (DOS) for a very narrow (7,0) and a larger (11,0) SWCNTs, whose structure and diameter most closely matches the e-beam engineered BG-SWCNT shown in Fig. 3b and c. Uniaxial compressive stress has been applied to the surface of the SWCNT to generate the flattening. Three values of the degree of flattening have been selected (Fig. 4 top): $f = 0$ corresponding to a pristine (7,0) SWCNT, $f = 0.15$ close to that of the structure shown in Fig. 3c, and the more compressed case of $f = 0.38$. It can be seen that the electronic structure of small diameter SWCNTs is significantly modified upon flattening.

Due to the increased curvature upon flattening (with the applied stress) the band gap of a (7,0) SWCNT is shown to be reduced from 0.5 eV for $f = 0$ to 0.1 eV for $f = 0.15$, and it eventually vanishes leading to nanotube metallization, as is in the model case of $f = 0.38$. The semiconductor-metal transition in semiconducting SWCNTs has been previously predicted for larger diameter SWCNTs [58,59] ((8,0) SWCNT and larger), and our results for a narrow (7,0) SWCNT are in agreement with these previous findings. Although the degree of flattening that can be achieved is not sufficient to reduce the band gap to zero, the sustained flattening creates regions of extreme strain, which are primarily responsible for the band gap change in the modified SWCNTs. In the proposed method to generate SWCNTs from bilayer graphene the degree of flattening does not change once the SWCNT has been formed, thus providing a nanostructure with pre-determined electronic properties, which can be exploited in future applications in small-scale nanodevices.

In larger diameter SWCNTs, the insulator-metal transition does not occur (Fig. 4 bottom) before the complete collapse

upon flattening, this behavior corresponds to the BG-SWCNT shown in Fig. 3b. Indeed, the semiconductor-metal transition occurs for an interlayer distance of 0.46 nm [58], whereas in the large flattened SWCNT formed from bilayer graphene the minor axis (depicted by blue delimiter in Fig. 3b) is 0.71 ± 0.02 nm. The SWCNTs formed from bilayer graphene have uniform height, that is, the minor axis does not vary significantly along the SWCNTs length.

4. Conclusions

In this work we have shown that by carefully choosing parameters of the 300 keV electron beam in scanning TEM mode, we can design BGNRs from BG. We produced constrictions in BGNRs when imaging at 80 keV, which formed SWCNT after further irradiation. By MD simulations we demonstrated that this SWCNT is flattened. Flattened SWCNTs are of much interest as the deformation and diameter on these nanostructures affect their electronic properties [54–59]. On the other hand, bilayer graphene has interesting electronic properties, which can also be tuned, e.g. opening of the band gap making BG semimetallic [60,61].

Acknowledgements

G.A.-S. acknowledges the support of CONACyT-DAAD stipend. E.B. acknowledges EPSRC Career Acceleration Fellowship, New Directions for EPSRC Research Leaders Award (EP/G005060) and ERC starting grant for funding. G.A.-S., U.K. and J.B. acknowledge the financial support by the DFG (German Research Foundation) and the Ministry of Science, Research and the Arts (MWK) of Baden-Wuerttemberg in the frame of the SALVE (Sub Angstrom Low-Voltage Electron Microscopy) project.

REFERENCES

- [1] Xu Z, Buehler MJ. Geometry controls conformation of graphene sheets: membranes, ribbons, and scrolls. *ACS Nano* 2010;4(7):3869–76.
- [2] Han MY, Özyilmaz B, Zhang Y, Kim P. Energy band-gap engineering of graphene nanoribbons. *Phys Rev Lett* 2007;98(20): 206805(4).
- [3] Chen Z, Lin Y-M, Rooks MJ, Avouris P. Graphene nano-ribbon electronics. *Phys E* 2007;40(2):228–32.
- [4] Cai J, Ruffieux P, Jaafar R, Bieri M, Braun T, Blankenburg S, et al. Atomically precise bottom-up fabrication of graphene nanoribbons. *Nature* 2010;466(7305):470–3.
- [5] Sidorov A, Mudd D, Sumanasekera G, Ouseph PJ, Jayanthi CS, Wu SY. Electrostatic deposition of graphene in a gaseous environment: a deterministic route for synthesizing rolled graphenes? *Nanotechnology* 2009;20(5): 055611(5).
- [6] Xie X, Ju L, Feng X, Sun Y, Zhou R, Liu K, et al. Controlled fabrication of high-quality carbon nanoscrolls from monolayer graphene. *Nano Lett* 2009;9(7):2565–70.
- [7] Son Y-W, Cohen ML, Louie SG. Half-metallic graphene nanoribbons. *Nature* 2006;444(7117):347–9.
- [8] Son Y-W, Cohen ML, Louie SG. Energy gaps in graphene nanoribbons. *Phys Rev Lett* 2006;97(21): 216803(4).
- [9] Nakada K, Fujita M, Dresselhaus G, Dresselhaus MS. Edge state in graphene ribbons: nanometer size effect and edge shape dependence. *Phys Rev B* 1996;54(24):17954–61.
- [10] Pisana S, Braganca PM, Marinero EE, Gurney BA. Tunable nanoscale graphene magnetometers. *Nano Lett* 2010;10(1):341–6.
- [11] Elias DC, Nair RR, Mohiuddin TMG, Morozov SV, Blake P, Halsall MP, et al. Control of graphene's properties by reversible hydrogenation: evidence for graphane. *Science* 2009;323(5914):610–3.
- [12] Cheng SH, Zou K, Okino F, Gutierrez HR, Gupta A, Shen N, et al. Reversible fluorination of graphene: evidence of a two-dimensional wide bandgap semiconductor. *Phys Rev B* 2010;81(20): 205435(5).
- [13] Robinson JT, Burgess JS, Junkermeier CE, Badescu SC, Reinecke TL, Perkins FK, et al. Properties of fluorinated graphene films. *Nano Lett* 2010;10(8):3001–5.
- [14] Stankovich S, Dikin DA, Piner RD, Kohlhaas KA, Kleinhammes A, Jia Y, et al. Synthesis of graphene-based nanosheets via chemical reduction of exfoliated graphite oxide. *Carbon* 2007;45(7):1558–65.
- [15] Dikin DA, Stankovich S, Zimney EJ, Piner RD, Dommett GHB, Evmenenko G, et al. Preparation and characterization of graphene oxide paper. *Nature* 2007;448(7152):457–60.
- [16] Gómez-Navarro C, Weitz RT, Bittner AM, Scolari M, Mews A, Burghard M, et al. Electronic transport properties of individual chemically reduced graphene oxide sheets. *Nano Lett* 2007;7(11):3499–503.
- [17] Tapasztó L, Dobrik G, Vertesy G, Lambin P, Biró LP. Tuning the electronic structure of graphene by ion irradiation. *Phys Rev B* 2008;78(23): 233407(4).
- [18] Chen JH, Cullen W, Jang C, Fuhrer M, Williams E. Defect scattering in graphene. *Phys Rev Lett* 2009;102(23): 236805(4).
- [19] Schedin F, Geim AK, Morozov SV, Hill EW, Blake P, Katsnelson MI, et al. Detection of individual gas molecules adsorbed on graphene. *Nat Mater* 2007;6(9):652–5.
- [20] Jung N, Kim N, Jockusch S, Turro NJ, Kim P, Brus L. Charge transfer chemical doping of few layer graphenes: charge distribution and band gap formation. *Nano Lett* 2009;9(12):4133–7.
- [21] Panchakarla LS, Subrahmanyam KS, Saha SK, Govindaraj A, Krishnamurthy HR, Waghmare UV, et al. Synthesis, structure, and properties of boron- and nitrogen-doped graphene. *Adv Mater* 2009;27(46):4726–30.
- [22] Pantelic RS, Suk JW, Hao Y, Ruoff RS, Stahlberg H. Oxidative doping renders graphene hydrophilic, facilitating its use as a support in biological TEM. *Nano Lett* 2011;11(10):4319–23.
- [23] Krasheninnikov AV, Banhart F. Engineering of nanostructured carbon materials with electron or ion beams. *Nat Mat* 2007;6(10):723–33.
- [24] Meyer JC, Geim AK, Katsnelson MI, Novoselov KS, Booth TJ, Roth S. The structure of suspended graphene sheets. *Nature* 2007;446(7131):60–3.
- [25] Fischbein MD, Drndić M. Electron beam nanosculpting of suspended graphene sheets. *Appl Phys Lett* 2008;93(11): 113107(3).
- [26] Song B, Schneider GF, Xu Q, Pandraud G, Dekker C, Zandbergen H. Atomic-scale electron-beam sculpting of near-defect-free graphene nanostructures. *Nano Lett* 2011;11(6):2247–50.
- [27] Krasheninnikov AV, Banhart F, Li JX, Foster AS, Nieminen RM. Stability of carbon nanotubes under electron irradiation: role of tube diameter and chirality. *Phys Rev B* 2005;72(12): 125428(6).
- [28] Pereira VM, Castro Neto AH, Liang HZ, Mahadevan L. Geometry, mechanics, and electronics of singular structures and wrinkles in graphene. *Phys Rev Lett* 2010;105(12): 156603(4).
- [29] Novoselov KS, Geim AK, Morozov SV, Jiang D, Zhang Y, Dubonos SV, et al. Electric field effect in atomically thin carbon films. *Science* 2004;306(5696):666–9.
- [30] Blake P, Castro Neto AH, Novoselov KS, Jiang D, Yang R, et al. Making graphene visible. *Appl Phys Lett* 2007;91(6): 063124(3).
- [31] Meyer JC, Girit CO, Crommie MF, Zettl A. Hydrocarbon lithography on graphene membranes. *Appl Phys Lett* 2008;92(12): 123110(3).
- [32] Gale JD, Rohl AL. The general utility lattice program (GULP). *Mol Simulat* 2003;29(5):291–341.
- [33] Brenner DW. Empirical potential for hydrocarbons for use in simulating the chemical vapor deposition of diamond films. *Phys Rev B* 1990;42(15):9458–71.
- [34] van Duin ACT, Dasgupta S, Lorant F, Goddard III WA. ReaxFF: a reactive force field for hydrocarbons. *J Phys Chem A* 2001;105(41):9396–409.
- [35] Clark SJ, Segall MD, Pickard CJ, Hasnip PJ, Probert MIJ, Refson K, et al. *Z Kristallogr* 2005;220(5–6):567–70.
- [36] Perdew JP, Wang Y. Pair-distribution function and its coupling-constant average for the spin-polarized electron gas. *Phys Rev B* 1992;46(20):947–54.
- [37] Ortmann F, Bechstedt F, Schmidt WG. Semiempirical van der Waals correction to the density functional description of solids and molecular structures. *Phys Rev B* 2006;73(20): 205101(10).
- [38] Liu Z, Suenaga K, Harris P, Iijima S. Open and closed edges of graphene layers. *Phys Rev Lett* 2009;102(1): 015501(4).
- [39] Huang JY, Ding F, Yakobson BI, Lu P, Qi L, Li J. In situ observation of graphene sublimation and multi-layer edge reconstructions. *Proc Nat Acad Sci USA* 2009;106(25):10103–8.
- [40] Meyer JC, Eder F, Kurasch S, Skakalova V, Kotakoski J, Park HJ, et al. An accurate measurement of electron beam induced displacement cross sections for single-layer graphene. *Phys Rev Lett* 2012;108(19): 196102(10).
- [41] Kotakoski J, Meyer JC, Kurasch S, Santos-Cottin D, Kaiser U, Krasheninnikov AV. Stone-wales-type transformations in

- carbon nanostructures driven by electron irradiation. *Phys Rev B* 2011;83(24): 245420(6).
- [42] Kotakoski J, Krasheninnikov AV, Kaiser U, Meyer JC. From point defects in graphene to two-dimensional amorphous carbon. *Phys Rev Lett* 2011;106(10): 105505(4).
- [43] Girit CO, Meyer JC, Erni R, Rossell MD, Kisielowski C, Yang L, et al. Graphene at the edge: stability and dynamics. *Science* 2009;323(5922):1705–8.
- [44] Mølhave K, Gudnason SB, Pedersen AT, Clausen CH, Horsewell A, Bøggild P. Electron irradiation-induced destruction of carbon nanotubes in electron microscopes. *Ultramicroscopy* 2007;108(1):52–7.
- [45] Rotkin SV, Gogotsi Y. Analysis of non-planar graphitic structures: from arched edge planes of graphite crystals to nanotubes. *Mat Res Innovations* 2002;5(5):191–200.
- [46] Banhart F. Irradiation effects in carbon nanostructures. *Rep Prog Phys* 1999;62(8):1181–221.
- [47] Chuvilin A, Kaiser U, Bichoutskaia E, Besley NA, Khlobystov AN. Direct transformation of graphene to fullerene. *Nat Chem* 2010;2(6):450–3.
- [48] Santana A, Zobelli A, Kotakoski J, Chuvilin A, Bichoutskaia E. Inclusion of radiation damage dynamics in high-resolution transmission electron microscopy image simulations: the example of graphene. *Phys Rev B* 2013;87(9): 094110(8).
- [49] Charlier JC, De Vita A, Blase X, Car R. Microscopic growth mechanisms for carbon nanotubes. *Science* 1997;275(5300):647–9.
- [50] Chopra NG, Benedict LX, Crespi VH, Cohen ML, Louie SG, Zettl A. Fully collapse carbon nanotubes. *Nature* 1995;377(6545):135–8.
- [51] Qi L, Yu JY, Feng J, Li J. In situ observations of the nucleation and growth of atomically sharp graphene bilayer edges. *Carbon* 2010;48(8):2354–60.
- [52] Discovery Studio Modeling Environment, Release 3.1, San Diego: Accelrys Software Inc., 2012.
- [53] Koch C. Determination of core structure periodicity and point defect density along dislocations. Arizona USA, Arizona State Univ, PhD thesis, 2002.
- [54] Yang L, Han J. Electronic structure of deformed carbon nanotubes. *Phys Rev Lett* 2000;85(1):154–7.
- [55] Gülseren O, Yildirim T, Ciraci S. Systematic ab initio study of curvature effects in carbon nanotubes. *Phys Rev B* 2002;65(15): 154401(15).
- [56] Fagan SB, da Silva LB, Mota R. Ab initio study of radial deformation plus vacancy on carbon nanotubes: energetics and electronic properties. *Nano Lett* 2003;3(3):289–91.
- [57] Clark SJ, Segall MD, Pickard CJ, Hasnip PJ, Probert MIJ, Refson K, et al. First principles methods using CASTEP. *Z Kristallogr* 2005;220(5–6):567–70.
- [58] Mazzoni MSC, Chacham H. Bandgap closure of a flattened semiconductor carbon nanotube: a first principles study. *Appl Phys Lett* 2000;76(12):1561–3.
- [59] Shan B, Lakatos GW, Peng S, Cho K. First-principles study of band-gap change in deformed nanotubes. *Appl Phys Lett* 2005;87(17): 173109(3).
- [60] Castro EV, Novoselov KS, Morozov SV, Peres NMR, Lopes dos Santos JMB, Nilsson J, et al. Biased bilayer graphene: semiconductor with a gap tunable by the electric field effect. *Phys Rev Lett* 2007;99(21): 216802(4).
- [61] Nilsson J, Castro Neto AH, Guinea F, Peres NMR. Electronic properties of bilayer and multilayer graphene. *Phys Rev B* 2008; 78(4): 045405(34).